From chaotic itinerancy to intermittent synchronization in complex networks

I. Leyva & Irene Sendiña-Nadal

Complex Systems Group & GISC, Universidad Rey Juan Carlos, 28933 Móstoles, Spain and Center for Biomedical Technology, Universidad Politécnica de Madrid, Pozuelo de Alarcón, 28223 Madrid, Spain

Christophe Letellier

Rouen Normandy University — CORIA, Avenue de l'Université, 76800 Saint-Etienne du Rouvray, France

R. Sevilla-Escoboza

Centro Universitario de los Lagos, Universidad de Guadalajara, Lagos de Moreno, Jalisco, Mexico

V. P. Vera-Ávila

Instituto Politécnico Nacional, Unidad Profesional Interdisciplinaria de Ingeniería Campus Guanajuato, Mexico

Although synchronization has been extensively studied, important processes underlying its emergence have remained hidden by the use of global order parameters. Here, we uncover how the route unfolds through a sequential transition between two well-known but previously unconnected phenomena: chaotic itinerancy (CI) and intermittent synchronization (IS). Using a new symbolic dynamics, we show that CI emerges as a collective yet unsynchronized exploration of different domains of the high-dimensional attractor, whose dimension is reduced as the coupling increases, ultimately collapsing back into the reference chaotic attractor of an individual unit. At this stage, the IS can emerge as irregular alternations between synchronous and asynchronous phases. The two phenomena are therefore mutually exclusive, each dominating a distinct coupling interval and governed by different mechanisms. Network structural heterogeneity enhances itinerant behavior since access to different domains of the attractor depends on the nodes' topological roles. The CI–IS crossover occurs within a consistent coupling interval across models and topologies. Experiments on electronic oscillator networks confirm this two-step process, establishing a unified framework for the route to synchronization in complex systems.

I. INTRODUCTION

The study of collective dynamics in complex networks has advanced our understanding of how local interactions give rise to emergent behaviors such as synchronization. criticality, and pattern formation. Among these, synchronization has been the main focus, particularly in strongly coupled systems where coherent global states emerge. This emphasis, however, has often obscured the dynamical richness of weakly coupled systems, which remain largely unexplored despite their relevance to many natural and artificial systems. The brain is the most prominent example, where the role of criticality has long been recognized, [1-4] but similar self-organized critical behavior has also been identified in other complex systems—from gene networks and ecosystems to artificial neural ensembles [5–7]. Operating near criticality allows such systems to balance robustness and sensitivity, maximizing adaptability and computational capacity [8].

When functioning away from global coherence, these systems display a rich repertoire of regimes and critical dynamics, including the two phenomena central to this work: chaotic itinerancy (CI) [9, 10] and intermittent synchronization (IS) [11, 12]. IS, observed at the edge of global synchronization, involves irregular alternations between coherent and unsynchronized phases [13, 14]. It corresponds to the well-known on-off intermittency [11, 12] and has been reported in neural activity under both healthy and epileptogenic conditions [15, 16].

IS thus provides a mechanism by which complex systems self-tune to operate near criticality, though its dependence on the underlying network structure remains poorly understood.

In contrast, CI refers to the trajectory within a high-dimensional attractor wandering through a sequence of metastable regimes (also called attractor ruins) connected [17–19] First introduced by Kaneko in nonequilibrium neural dynamics [20], CI has been observed in diverse contexts, including sensory processing in the olfactory cortex [10], perceptual switching in EEG activity [21], laser dynamics [22, 23], and adaptive robotic behavior [24–27]. In neural systems, metastable itinerant dynamics are thought to underlie cognitive processes such as working memory, decision making, and behavioral flexibility.[28–33]

These features have also made CI relevant to machine learning and computation. Reservoir computing, for instance, exploits high-dimensional transients for memory and pattern classification, and recent work has demonstrated controlled CI in such architectures [34–37]. This supports the idea that transient, metastable dynamics are essential for flexible and context-dependent computation in both biological and artificial systems [19, 32, 33, 38].

Despite extensive studies of CI in globally coupled or random networks [9, 20, 35, 37, 39], its relationship with network topology remains poorly understood. Yet realworld systems exhibiting CI often feature modular, hierarchical, or heterogeneous architectures [19, 40, 41].

The main goal of this work is to address this gap. Specifically, we investigate how network topology influences the emergence, organization, and persistence of chaotic itinerancy in weakly coupled oscillator systems, and clarify its connection with IS, as the two phenomena are often confounded [42]. We show that CI and IS are successive, mutually exclusive stages along the route to synchronization, each associated with distinct critical behaviors. These properties are robust across topologies, network sizes, node dynamics, and are further confirmed experimentally in electronic oscillator networks.

To track CI, we introduce a new symbolic dynamics approach that encodes nodal trajectories into symbolic sequences, capturing transitions with greater sensitivity than standard time-averaged measures. This framework allows the node-level analysis of visiting sequences and reveals how topological roles modulate access to different nodal regimes. It thus provides new insight into how the network topology shapes dynamics in complex dynamical systems —bridging a gap between network theory and nonlinear dynamics, may prove useful for understanding the computational and decision processes driven by chaotic itinerancy.

II. CHAOTIC ITINERANCY AND INTERMITTENT SYNCHRONIZATION

The characterization of the route to synchronization in coupled oscillator networks is often described in terms of global, time-averaged metrics, such as the mean synchronization error or an order parameter that summarizes collective coherence. However, such global indicators often hide the underlying, time-dependent phenomena occurring at the nodal level. In particular, they hide two critical yet interconnected processes: chaotic itinerancy (CI) and intermittent synchronization (IS). CI corresponds to irregular transitions at the node level among metastable regimes, whereas IS manifests as intermittent alternations between synchronous and asynchronous phases at the network scale. Both arise in weak-to-intermediate coupling values, revealing the multiscale organization of dynamics that bridges nodal and network levels of the synchronization process.

To explore these regimes, we consider a network of N diffusively coupled identical chaotic oscillators governed by

$$\dot{\boldsymbol{x}}_i = \mathbf{f}(\boldsymbol{x}_i) - d \sum_{j=1}^N L_{ij} \, \mathbf{h}(\boldsymbol{x}_j)$$
 (1)

where $\mathbf{x}_i \in \mathbb{R}^m$ is the state vector of the *i*th node, \mathbf{f} and \mathbf{h} are $\mathbb{R}^m \to \mathbb{R}^m$ functions governing the intrinsic dynamics of an isolated unit and the coupling between them respectively; d is the coupling strength, L_{ij} is the Laplacian matrix encoding the network topology, with

 $L_{ij} = -1$ if nodes i and j are connected ($L_{ij} = 0$ otherwise), and $L_{ii} = k_i$ is the degree of the ith node. This framework captures a broad class of diffusive interactions and allows us to systematically track the underlying multiscale organization of the synchronization process. The network is a single dynamical system whose state space is \mathbb{R}^{Nm} , and producing an attractor $\mathcal{A}(d) \subset \mathbb{R}^{Nm}$ depends on the coupling value d, the other parameter values being kept constant. Indeed, each node i is associated with a m-dimensional sub-state space \mathbb{R}^m_i in which there is an attractor $\mathcal{A}_i(d) \subset \mathbb{R}^m_i$. When uncoupled d = 0, the sub-attractors $\mathcal{A}_i(0)$ are identical to \mathcal{A}_r that will be in the next Sections named as the reference attractor.

Figure 1 illustrates the emergence of the two dynamical phenomena discussed above. Panel (a) shows the expected gradual decrease of the synchronization error

$$\langle E \rangle = \lim_{T \to \infty} (1/T) \int_0^T E(t) dt,$$
 (2)

with $E(t) = \frac{2}{N(N-1)} \sum_{i < j} \|\mathbf{x}_i(t) - \mathbf{x}_j(t)\|^2$, for a network of N = 100 diffusively coupled Rössler oscillators.

Along this synchronization process, two key phenomena are typically overlooked: at low coupling [red dot at d=0.08, Fig. 1(b)], CI dominates, here represented by the trajectories of two arbitrary nodes (we plot the maxima of their two x-variables, vertically shifted for clarity). At higher couplings [blue square at d=0.28 in Fig. 1(c)], IS becomes the dominant feature, where the instantaneous synchronization error E(t) exhibits intervals of near-perfect synchrony interrupted by desynchronization bursts [Fig. 1(c)].

Further examples shown in Fig. 1(d) for a small complete graph of Lorenz oscillators and in Fig. 1(e) a network of globally coupled Logistic maps [20], confirm the generality of these behaviors across different models and network structures.

These observations underscore the need for analytical tools that outperform ensemble-averaged measures and can capture the multiscale nature of these phenomena along the synchronization process. In the following subsections, we introduce two dedicated metrics: the CI and IS indexes.

A. Chaotic itinerancy index

Quantifying chaotic itinerancy (CI) in a network dynamics is challenging due to the high-dimensional wandering trajectories [9, 17, 18]. Previous attempts relied on Lyapunov exponents, recurrent plots or entropy rates to detect transitions between metastable regimes [21, 30, 41–43]. However, most of these approaches rely on global or averaged measures, thus overlooking the heterogeneous and node-dependent nature of transitions in networked systems. In order to overcome this limitation, we introduce a symbolic dynamics that captures CI directly at the nodal level, tracking the time sequence of

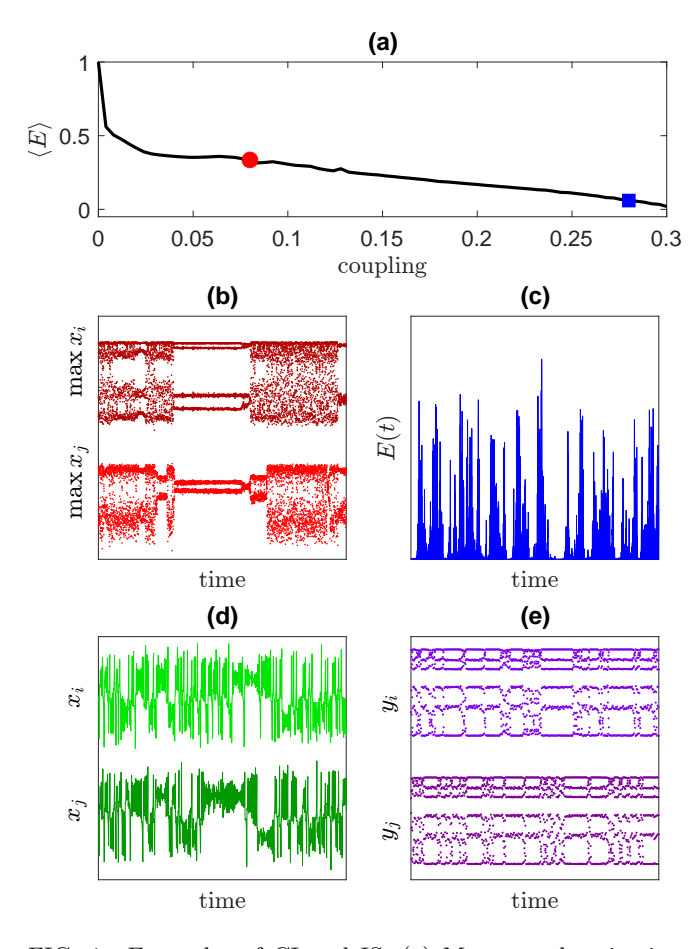


FIG. 1. Examples of CI and IS. (a) Mean synchronization error $\langle E \rangle$ of a network of Rössler units, highlighting two points along the route to synchronization: the red dot marking a coupling regime where chaotic itinerancy (CI) takes place, and at higher coupling, the blue square pointing out a regime of intermittent synchronization (IS). (b) Evidence of the CI marked as a red point in (a) (d = 0.08), showing the maxima of the x variable of two arbitrary nodes in the network (shifted for visualization). (c) Evidence of the IS marked as a blue square in (a) (d = 0.28) using the instantaneous synchronization error E(t). (d) Example of CI showing the x variable (shifted for clarity) of two arbitrary Lorenz nodes from a larger clique configuration. (e) Globally coupled N=100 logistic maps as an example of a discrete dynamical system showing CI. Models used in Eq. (1): (a) and (b) N = 100 Rössler nodes coupled in a scalefree configuration with average node degree $\langle k \rangle = 4$, with $\mathbf{f}(\mathbf{x}) = [-y - z, x + ay, z(x - 4) + 2] \text{ and } \mathbf{h}(\mathbf{x}) = [0, y, 0],$ with a = 0.432; (d) a clique graph of N = 5 Lorenz systems with $\mathbf{f}(\mathbf{x}) = [-10(y-x), x(28-z) - y, xy - 2z], \mathbf{h}(\mathbf{x}) =$ [0, y, 0]. Parameters used in (d) for globally coupled Logistic maps, $y_i(t+1) = f\left((1-d)y_i(t) + \frac{d}{N}\sum_{j=1}^{N} y_j(t)\right)$ with $f(x) = 4(1-x^2)$ and d = 0.1.

transitions for each node individually. The goal is to reduce each oscillator's time series to a discrete set of symbols that reflect the sequence of regimes over time, enabling us to detect and quantify transitions between them. The process is exemplified in Fig. 2 for two nodes

of the N=100 Rössler oscillators network.

Let $X_i = \{X_i(t_p)\}_{p=1}^P$ denote the scalar time series associated with the ith node, extracted from its state vector x_i at discrete times t_p . The choice of variable and sampling strategy can be adapted to the system under study. In the Fig 2 example, each node's time series is obtained by sampling the local maxima of the first variable, i.e. the $X_i = x_i$ are the crossings of a Poincaré section defined by $\mathcal{P}_i \equiv \{(x_i \in \mathbb{R} \mid \dot{x}_i = 0, x_i > 0\}$. The series is normalized to the interval [0,1] as $\hat{X}_i = X_i/\max(X_i)$, ensuring comparability across nodes and realizations.

Note that, for other dynamical systems or data, regular time sampling or local extrema of other variables can be used. The method does not rely on a specific type of sampling, as long as it captures relevant dynamical features. We will present examples in the next Sections.

The normalized data are partitioned into N_{τ} time windows of D consecutive samples each, and into N_{β} equally spaced amplitude bins. Each cell of this space-time grid is labeled by the indices (τ, β) , where $\tau \in \{1, \ldots, N_{\tau}\}$ and $\beta \in \{1, \ldots, N_{\beta}\}$. In the example given in Fig. 2(a,b), $N_{\beta} = 6$, and only 20 time windows are shown from a much larger N_{τ} . The window size D has to be chosen such that there is a trade-off between capturing shortlived transitions with adequate time resolution and ensuring statistical reliability of the symbolic dynamics. Similarly, the number of amplitude bins N_{β} is set to discretize the state-space exploration with sufficient granularity, while remaining robust to moderate changes; as later illustrated, the results are not critically sensitive to the specific choice of D or N_{β} (see Suppl. Material, Fig. S1).

A (τ, β) cell is considered visited if the number of points $\pi_{\tau,\beta}^{(i)}$ falling inside exceeds a threshold θ :

$$\Pi_{\tau,\beta}^{(i)} = \begin{cases} 1, & \text{if } \pi_{\tau,\beta}^{(i)} > \theta, \\ 0, & \text{otherwise.} \end{cases}$$
(3)

Figure 2(c,d) illustrates this binary visitation grid for the two series in panels (a) and (b), respectively, where yellow encodes a visited cell and blue a non-visited one.

The symbolic state of node i in window τ is then defined as the number of visited cells

$$\sigma_{\tau}^{(i)} = \sum_{\beta=1}^{N_{\beta}} \Pi_{\tau,\beta}^{(i)} \tag{4}$$

as shown in Figs. 2(e,f). This symbolic dynamics $\sigma_{\tau}^{(i)} \in \{1,\ldots,N_{\beta}\}$ encodes the part of the attractor visited for that duration. Large values of $\sigma_{\tau}^{(i)}$ correspond to a trajectory exploring wide domains of the attractor, whereas small values indicate confinement to near-periodic or low-developed chaotic regimes.

Applying this procedure to all nodes and time windows yields a *symbolic raster plot* $\sigma = \{\sigma_{\tau}^{(i)}\}$ (Fig. 2(g)), which captures the nodal diversity and time variability of the network's dynamics.

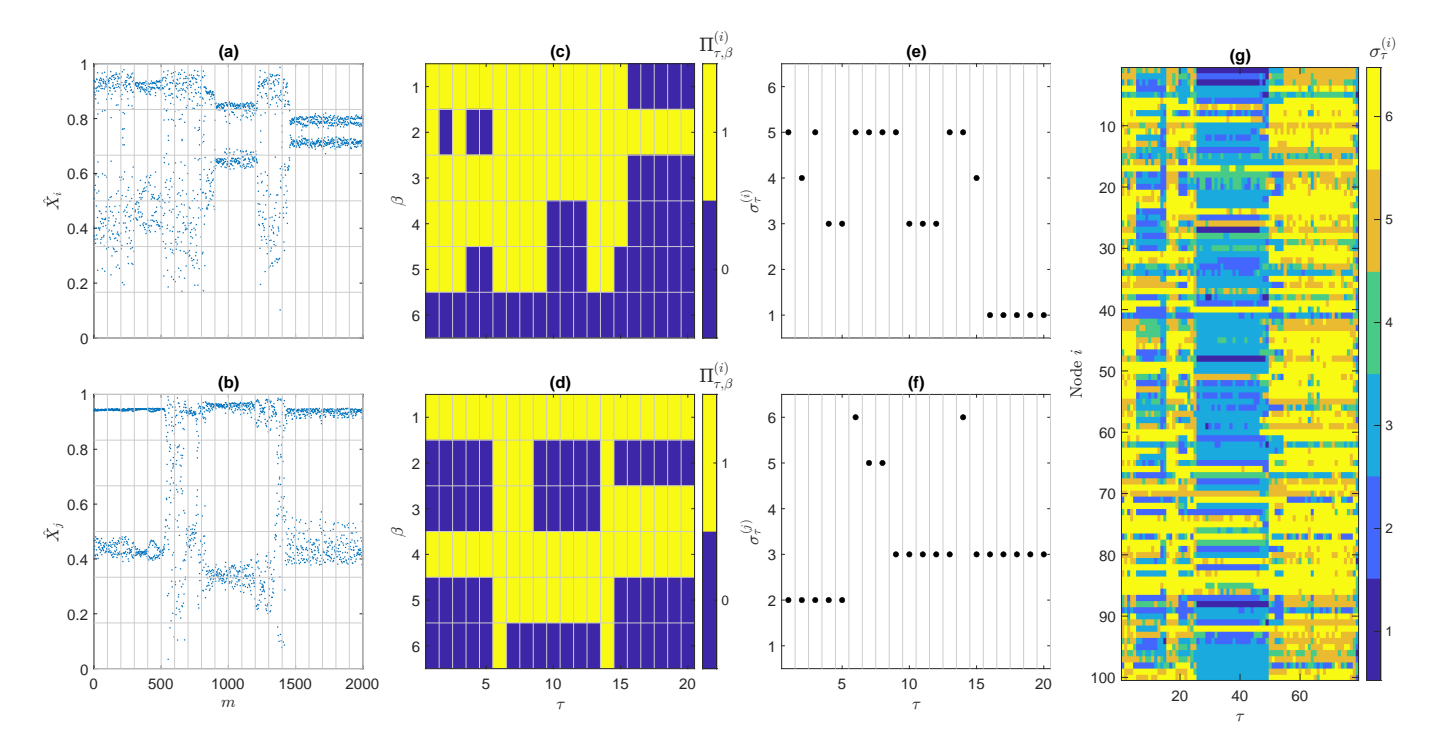


FIG. 2. Symbolic encoding procedure used to characterize chaotic itinerancy, illustrated for two arbitrary nodes in a network of coupled Rössler oscillators. (a, b) Normalized sampled time series \hat{X}_i and \hat{X}_j , corresponding to the scalar variables $X_i(t)$ and $X_j(t)$ of two arbitrary nodes, obtained here as the sequence of maxima of the Rössler variable x. The data points are distributed over a grid (gray lines) composed of $N_{\tau} \times N_{\beta}$ cells, where each time window τ contains D consecutive samples. In this example, D = 100 and only 20 time windows (out of the total N_{τ}) are shown. (c, d) Binary occupancy maps $\Pi_{\tau,\beta}^{(i)}$ for the nodes shown in panels (a) and (b). Each cell (τ,β) is marked as visited $(\Pi_{\tau,\beta}^{(i)} = 1$, yellow) if it contains more than $\theta = 2$ points, and as empty $(\Pi_{\tau,\beta}^{(i)} = 0$, blue) otherwise. (e, f) Symbolic state $\sigma_{\tau}^{(i)}$ for each time window, defined as the number of active cells visited by node i during window τ . In the example, full exploration of the spatial partition corresponds to $\sigma_{\tau}^{(i)} = N_{\beta} = 6$. (g) Symbolic raster plot $\sigma = \{\sigma_{\tau}^{(i)}\}$ showing the symbolic evolution of all N nodes in the network. Example shown corresponds to a scale-free (SF) network of N = 100 coupled Rössler oscillators with coupling strength d = 0.08 and parameter a = 0.432.

The *chaotic itinerancy index* is then defined as the average number of transitions between symbolic states per node and per window:

$$\Phi_{\sigma} = \frac{1}{N(N_{\tau} - 1)} \sum_{i=1}^{N} \sum_{\tau=1}^{N_{\tau} - 1} \left[1 - \delta_{\sigma_{\tau+1}^{(i)}, \sigma_{\tau}^{(i)}} \right], \tag{4}$$

where δ_{ab} is the Kronecker delta. High values of Φ_{σ} indicate frequent transitions between metastable regimes—strongly itinerant trajectory—whereas small values reflect a single regime.

B. Intermittent Synchronization Index

In contrast to chaotic itinerancy, the quantification of intermittent synchronization (IS) is a more established problem. On-off intermittence has been extensively studied in low-dimensional and small ensembles of coupled chaotic systems [13, 44], but the intermittence in complex networks has not been explored as much [11, 12]. Several approaches have been proposed to characterize this behavior, typically based on the statistics of laminar-phase

durations, return maps, or burst amplitude distributions [14, 45]. Here, rather than introducing a new intermittency measure, we adopt a normalized definition that mirrors the structure of the CI index.

While Φ_{σ} quantifies CI by accounting for local transitions between metastable regimes, the equivalent *intermittent synchronization index* Φ_{E} should capture global alternations between coherent and incoherent network phases defining IS.

It is computed from the instantaneous synchronization error E(t) introduced above. We binarize E(t) using a threshold θ_E , defining $\varepsilon(t) = H(E(t) - \theta_E)$ where H(x) is the Heaviside step function [11, 46]. The value $\varepsilon(t) = 0$ corresponds to (synchronous) phases, while $\varepsilon(t) = 1$ denotes desynchronized bursts. Typical practical choices for the threshold are small (e.g. $\theta_E \sim 10^{-5}$), but θ_E should be set according to noise level.

The index is then defined as the normalized number of transitions between these two symbols:

$$\Phi_E = \frac{1}{2} \frac{1}{T - 1} \sum_{t=1}^{T - 1} |\varepsilon(t + 1) - \varepsilon(t)|$$
 (5)

Large values of Φ_E indicate frequent switching between coherent and non-coherent phases —signatures of on-off intermittency— whereas $\Phi_E=0$ corresponds either to complete incoherence or full synchronization. Thus, Φ_E measures the instability of the laminar phases rather than the absolute level of coherence. Both indices, Φ_σ and Φ_E , provide complementary quantitative descriptions of the nodal level (CI) and network level (IS) dynamics that organize the route to synchronization in complex networks.

III. SEQUENTIAL ONSET OF CI AND IS

To investigate the onset and development of chaotic itinerancy and its relation to intermittent synchronization, we analyze the route to synchronization of an N=100 ensemble of identical Rossler oscillators in a heterogeneous undirected topology with $\langle k \rangle =4$. Such a topology exhibits a sufficient degree of heterogeneity and is large enough to avoid the appearance of global periodic regimes, allowing us to focus on the genuinely chaotic itinerant dynamics that emerge during the route to synchronization. Statistical robustness is achieved by sampling a large number of different initial conditions for the oscillator states.

Figure 3(a) reports the evolution of the CI index Φ_{σ} (red) and the IS index Φ_{E} (blue) as a function of the coupling strength d, together with the synchronization error E (in green) plotted as a reference frame of the global coherence state. The key insight is that Φ_{σ} and Φ_{E} are activated consecutively and do not coexist: itinerancy is established immediately at low couplings and increases rapidly, reflecting the onset of a collective exploration of metastable regimes. The CI index reaches a maximum and then fades progressively as the oscillators converge onto the same symbolic state, corresponding to the reference chaotic attractor \mathcal{A}_{r} .

Only after this contraction, IS does emerge as a signal that the final stage of the synchronization process has begun (around $d \sim 0.2$ in the example). During the IS regime, periods of near-synchrony are interrupted by global desynchronization bursts, in line with previous findings [11, 46]. Here, its role is reinterpreted as the natural continuation of the CI collapse, where all the nodes settled in the reference attractor $\mathcal{A}_{\rm r}$ but not in a synchronous way. The sequencing of these two dynamical regimes — first CI, then IS— is a central contribution of this work.

A complementary view of the sequential onset of CI and IS comes from the Lyapunov spectrum of the full 3N-dimensional system. We computed the spectrum using the standard Benettin algorithm [47] with Gram–Schmidt reorthonormalization on the tangent space of the network dynamics, following the procedure of Ref. [48]. The N largest Lyapunov exponents are shown in Fig. 3(a) (shaded gray) overlaid on the CI and IS indicators. CI persists while the exponents λ_N through λ_4 become negative sequentially, indicating the

progressive loss of effective dimension that enabled wandering through different regimes. When λ_4 reaches zero [around $d \sim 0.22$ in the example; see inset in Fig. 3(a)], CI collapses, signaled by the vanishing of Φ_{σ} . At that point, the synchronization process can begin, and the IS index Φ_{σ} increases as the system fluctuates near the synchronous manifold due to the only remaining marginal direction given by $\lambda_3 \sim 0$. The final collapse occurs when simultaneously $\lambda_3 < 0$ and $\lambda_2 = 0$, leaving $\mathcal{A}(d)$ being topologically equivalent to $\mathcal{A}_{\rm r}$.

Equivalently, from the Lyapunov spectrum we can use the Kaplan-Yorke conjecture to calculate the Lyapunov dimension of the whole attractor as a function of the coupling, $\mathcal{D}_L(d)$ [49]. From this point of view, CI takes place in the interval $\mathcal{D}_L(0) = N\mathcal{D}_r > \mathcal{D}_L(d) > 4$, where $\mathcal{D}_r = 2.03$ is the Lyapunov dimension of \mathcal{A}_r for the chosen parameters. Then, IS is observed in the sequent interval $4 \geqslant \mathcal{D}_L(d) \geqslant \mathcal{D}_r$. According to this Rössler network, chaotic itinerancy is only observed when the dynamics can be embedded in a space whose dimension is at least equal to 5.

The correlation between the presence of near-zero Lyapunov exponents and the occurrence of chaotic itinerancy (CI) or intermittent synchronization (IS) has been discussed in previous works [17, 43, 50–52], but a clear distinction between these two regimes and their specific correspondence with the Lyapunov spectrum in large-scale systems had not been clearly established.

To assess the presence of criticality in CI and IS, we analyze the distribution of residence durations within the symbolic state corresponding to the reference attractor \mathcal{A}_{r} , encoded by the highest symbolic value $\sigma_{i}^{\tau} = N_{\beta}$. We therefore measure, for each node, the residence duration n_{τ} during which it remains in N_{β} before switching onto another symbol. Figure 3(b) shows that the resulting distribution —averaged over all nodes and realizations— follows a power-law decay, $P(n_{\tau}) \sim n_{\tau}^{-1.7}$, for d approaching 0.22, the coupling value at which CI ceases. The emergence of this scaling precisely at the point where the itinerant dynamics collapse supports the interpretation of a critical transition: as the nodes diminish their exploration of different regimes, its time organization becomes scale-free. Similar power-law residenceduration distributions have been reported in deterministic [42] and stochastic [53] models of chaotic itinerancy. where nodal trajectories wander among different regimes, although without explicitly identifying this final critical stage.

An analogous analysis was performed for the intermittent synchronization. Here, the relevant residence time corresponds to the duration of the synchronized phases, defined as the intervals during which the global synchronization error E(t) remains below a small threshold before a desynchronization burst occurs. Figure 3(c) shows that the distribution of these synchronized phases durations t_{ℓ} [measured at d=0.27, blue circle in Fig. 3(a)] follows a power-law scaling, $P(t_{\ell}) \sim t_{l}^{-1.5}$, consistent with the universal exponent reported for on–off intermittency

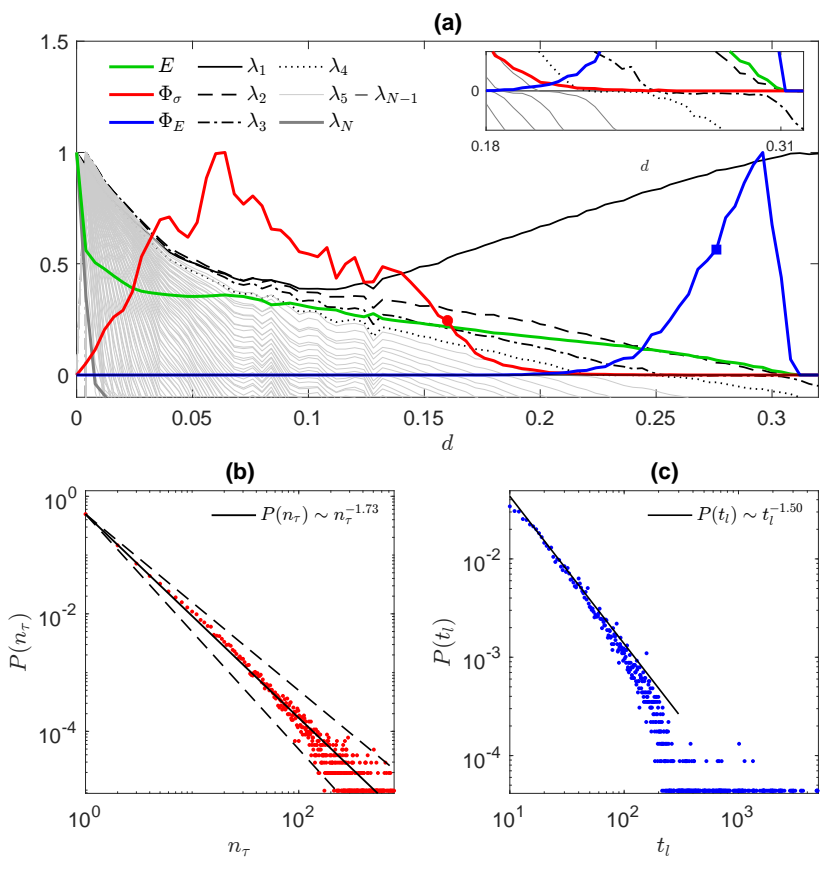


FIG. 3. Synchronization route and emergence of chaotic itinerancy (CI) and intermittent synchronization (IS) in a network of N=100 chaotic Rössler oscillators. (a) Global synchronization error E (green), chaotic itinerancy index Φ_{σ} (red), and intermittent synchronization index Φ_{E} (blue) as a function of the coupling strength d. The N largest Lyapunov exponents are also plotted with different colors of gray and line styles as indicated in the legend. The inset zooms the coupling interval where CI vanishes and gives rise to IS until the system reaches global synchrony with $\lambda_1 > 0$, $\lambda_2 = 0$, $\lambda_3 < 0$. (b) Log-log probability distribution of the residence duration n_{τ} in the most developed chaotic symbolic state $\sigma = N_{\beta}$, at d = 0.16, red circle in (a), showing power-law behavior. The solid straight-line shows the best fit to a power law $P(n_{\tau}) \sim n_{\tau}^{-1.73}$, and the dashed straight-lines bounding the data correspond to exponents 2 (upper) and 1.5 (bottom). (c) Log-log probability distribution of the coherent phase durations t_{ℓ} during IS, at d = 0.27 (blue square in (a)), following a $P(t_{\ell}) \sim t_{\ell}^{-3/2}$ scaling typical of on-off intermittency. Ensemble averages are computed over 30 independent realizations of initial conditions. Rest of parameters: D = 200, $N_{\beta} = 6$, $\theta = 3$. The network structure is an instance of a network with scale-free degree distribution and average degree 4.

[13, 14, 54–56].

To further assess the consistency of the CI-IS sequence, we compared systems with different network architectures and node dynamics. Specifically, we analyzed networks with degree distributions ranging from complete graph to power-law, system sizes from N=5 to N=500 nodes, and distinct oscillator models by including the Lorenz system. Additionally, in this last case the analyzed data is not a Poincaré section, but a regular periodic sampling of the time series of the x variable of the nodes, with D=100 and $N_{\beta}=2$, adapted to the different time scale and nature of the state space.

Figure 4 shows that when the coupling strength d is rescaled by the corresponding critical synchronization threshold d_c of each system, the crossover between the itinerant and intermittent phenomena, identified by the intersection of Φ_{σ} and Φ_{E} , occurs at approximately

 $d/d_c \simeq 2/3$ in all cases. This robust scaling suggests a general organizational principle in the route to synchronization: independently of the nodal dynamics or network topology, the system transitions from locally itinerant to globally intermittent dynamics at the same point of the route to coherence.

IV. CI NODAL STRUCTURE

The symbolic dynamics introduced in Sec. II A not only provides a quantitative characterization of chaotic itinerancy but also enables a detailed exploration of how the nodal structure of the network shapes chaotic itinerancy. By encoding each node's trajectory into N_{β} symbols, we can directly assess how structural heterogeneity modulates the access and persistence of nodes within dis-

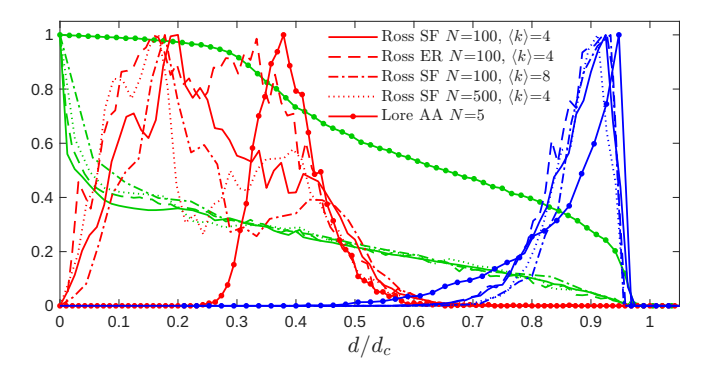


FIG. 4. Comparison of the chaotic itinerancy index Φ_{σ} (red) and intermittent synchronization index Φ_{E} (blue) for different combinations of network structures, sizes, and dynamical systems, distinguished by linestyles as indicated in the legend. The corresponding synchronization error E (green) is also shown. In all cases, the coupling strength d is normalized by the critical synchronization threshold d_{c} of each network. Remarkably, despite the diversity of systems, the crossover point consistently occurs at $d/d_{c} \approx 2/3$.

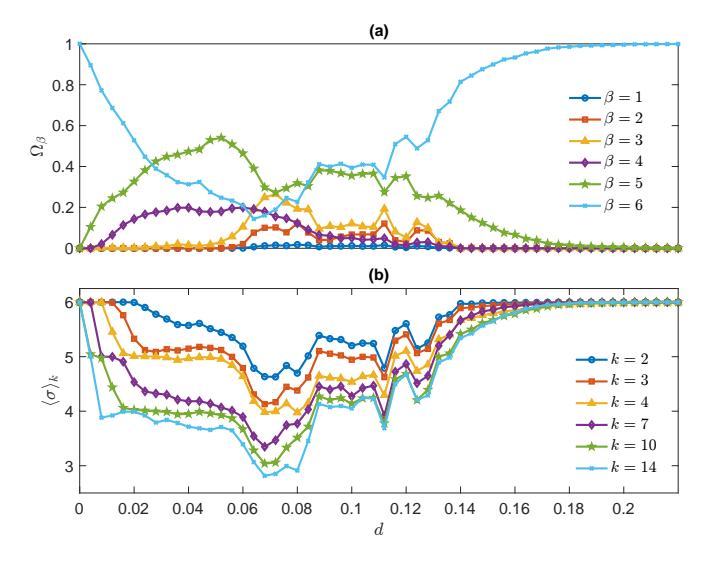


FIG. 5. Analysis of the symbolic state realization for the network used in Fig. 3. (a) Realization probability of symbol Ω_{β} for each symbol $\beta = 1, \ldots, N_{\beta} = 6$, and (b) average symbolic state per degree class $\langle \sigma \rangle_k$ as a function of coupling d.

tinct regimes of the attractor $\mathcal{A}(d)$.

Figure 5(a) illustrates how the symbolic occupation statistics evolve across the coupling range where CI develops. The *symbol probability*

$$\Omega_{\beta} = \frac{1}{NN_{\tau}} \sum_{\tau=1}^{N_{\tau}} \sum_{i=1}^{N} \delta_{\sigma_{\tau}^{(i)},\beta}, \tag{6}$$

quantifies the relative frequency of each symbol $\beta \in \{1,\ldots,N_\beta\}$ across all nodes and time windows. For d=0, the highest symbolic state $\beta=N_\beta$ is the only one to be observed. As d increases, additional symbols — representing more regular and less developed regimes — become progressively visited. Each symbol reaches its max-

imum realization at a specific coupling value [Fig. 5(a)], revealing a hierarchical ordering in which less chaotic regimes peak later along the route to synchronization. As d approaches the critical value at which Φ_{σ} collapses $(d \sim 0.22)$, the distribution reconverges toward $\Omega_{N_{\beta}} \approx 1$, indicating that CI has effectively ceased.

Figure 5(b) reveals clear evidence of topologically induced dynamical differentiation [57, 58]. We define the degree-class symbolic average as

$$\langle \sigma \rangle_k = \frac{1}{|C_k|N_\tau} \sum_{i \in C_t} \sum_{\tau=1}^{N_\tau} \sigma_\tau^{(i)}, \tag{7}$$

where C_k is the set of nodes with degree k. The results indicate that the regimes accessible to each node depends strongly on its topological role. Highly connected nodes (hubs) explore a larger set of regimes and settle earlier into less chaotic ones, whereas low-degree nodes remain mostly confined in regimes close to the original chaotic regime. This degree-dependent differentiation produces a clear hierarchy in symbol exploration, linking topological heterogeneity to dynamical specialization during the collapse of itinerancy.

This degree-dependent differentiation may have broader implications for understanding how itinerance organize and interact in heterogeneous systems such as large-scale brain dynamics or in the design of reservoir computing architectures, where structured heterogeneity enhances computational flexibility and memory capacity.

Functional symbolic synchronization

The symbolic representation introduced above is not limited to quantifying CI, but it provides a new tool to uncover patterns of coordination that remain hidden to other approaches based on instantaneous phase or amplitude correlations. This perspective allows us to define a *symbolic synchronization*, where nodes coordinate their dynamics even in the absence or other forms of synchrony. We thus examine the extent to which nodes undergo coordinated symbolic transitions, and how it correlates with their structural roles.

Figure 6(a) shows the functional symbolic synchronization matrix, S_{σ} , for the same ensemble of oscillators analyzed in Sec. III computed at a representative coupling within the chaotic itinerancy regime (d=0.024). Each matrix element is the normalized Hamming correlation of the respective symbolic sequences:

$$S_{\sigma}^{(i,j)} = \frac{1}{N_{\tau}} \sum_{\tau=1}^{N_{\tau}} \delta_{\sigma_{\tau}^{(i)}, \sigma_{\tau}^{(j)}}.$$
 (8)

High $S_{\sigma}^{(i,j)}$ values indicate frequent symbolic coordination, even in the absence of direct signal synchronization.

The resulting patterns reveal that nodal symbolic synchronization can emerge well before global phase locking, uncovering latent forms of coordination driven by

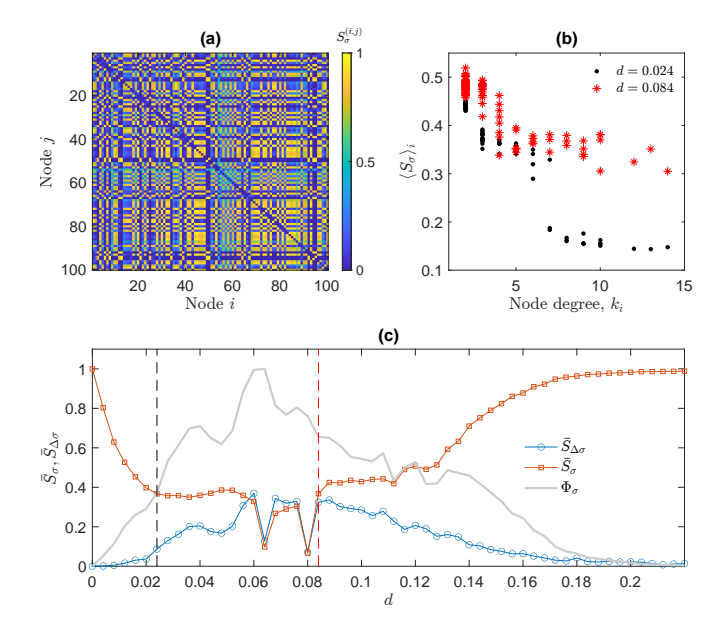


FIG. 6. (a) Functional symbolic synchronisation matrix $S_{\sigma}^{(i,j)}$ for the same network ensemble used in Fig. 3 for d=0.024. (b) Average functional symbolic synchronisation of each node with its neighbours, $\langle S_{\sigma} \rangle_i$, as a function of their degree k_i for two coupling values shown as vertical lines in panel (c). (c) Global averages of symbolic state synchronization, \bar{S}_{σ} , and jump state synchronization, $\bar{S}_{\Delta\sigma}$, versus coupling d. Chaotic itinerancy index Φ_{σ} is plotted in gray for reference.

the network that can offer information over the underlying topology, even for very weak couplings. Figure 6(b) displays the average symbolic synchronization of each node with its neighbors, $\langle S_{\sigma} \rangle_i = N^{-1} \sum_j S_{\sigma}^{(i,j)}$, as a function of its degree k_i for two representative coupling strengths [marked by vertical lines in Fig. 6(c)]. The observed monotonic decrease of $\langle S_{\sigma} \rangle_i$ with k_i indicates that hubs synchronize less their regimes than low-degree nodes, which is a reflection of the degree-dependent range of symbol exploration [Fig. 5(b)].

However, as we have shown before, we can describe another possible level of coordination in the weakly coupled regime: the *itinerancy synchronization*, where nodes change their symbols simultaneously. To disentangle this process from the symbolic synchronization we also compute

$$S_{\Delta\sigma}^{(i,j)} = \frac{1}{N_{\tau} - 1} \sum_{\tau=1}^{N_{\tau} - 1} \delta_{\Delta\sigma_{\tau}^{(i)}, 1} \delta_{\Delta\sigma_{\tau}^{(j)}, 1}, \tag{9}$$

where $\Delta \sigma_{\tau}^{(i)} = |\sigma_{\tau+1}^{(i)} - \sigma_{\tau}^{(i)}|$ that indicates whether node i presents symbol switched between consecutive windows. This quantity captures whether nodes perform synchronous symbol switches, regardless of which state they occupy before or after the transition. To compare the two types of synchronization, Fig. 6(c) shows the evolution as a function of the coupling of the mean values of the matrices given by Eqs.(8) and (9), \bar{S}_{σ} and $\bar{S}_{\Delta\sigma}$ respectively.

tively. In the CI regime (Φ_{σ} is also plotted as a reference), $\bar{S}_{\Delta\sigma}$ rises sharply, showing that transitions become temporally aligned across the network, even though \bar{S}_{σ} stays lower because nodes often realize different symbols. At the end of CI, \bar{S}_{σ} becomes high again, as all nodes converge to the same symbol, while $\bar{S}_{\Delta\sigma}$ returns to zero since the transitions end. It provides a functional viewpoint on how coherence develops in complex networks as a process with several stages: first, nodes synchronize the timing of regime switches (transition synchrony), and later they stabilize into the same symbols (state synchrony).

V. EXPERIMENTAL EVIDENCE

To experimentally test our predictions, we built a hybrid electronic network composed of N=28 analog oscillators emulating Rössler-like chaotic dynamics. The oscillators are interconnected through resistive links that enable adjustable diffusive coupling, with the effective coupling strength d controlled externally by a programmable voltage source. All signal acquisition and feedback operations are handled by a real-time control platform (National Instruments CompactRIO) equipped with high-resolution data acquisition, ensuring precise monitoring and tuning of the local and collective dynamics.

This hybrid architecture allows precise and repeatable control of the coupling strength, as well as arbitrary reconfiguration of the network connectivity. In the present study, we used N=28 networks generated according to the Watts–Strogatz model [59] with an average degree $\langle k \rangle = 4$ and two levels of randomness: p=1, corresponding to an Erdős–Rényi–like topology, and p=0.1, which preserves some clustering while remaining largely random. Figure 7 summarizes the experimental platform and real-time control scheme, while additional details are provided in the Supplementary Information.

Figure 8 presents the experimental measurements of the chaotic itinerancy index Φ_{σ} , the intermittent synchronization index Φ_{E} , and the average synchronization error E as a function of the applied coupling for the two implemented topologies. Although the experimental error E remains finite due to noise and component mismatch, both indices display a clear and robust crossover: at low coupling $\Phi_{\sigma} > \Phi_{E}$ (itinerant-dominated dynamics), while at stronger coupling $\Phi_{E} > \Phi_{\sigma}$ (intermittency-dominated dynamics). These observations confirm that the sequence of chaotic itinerancy and intermittent synchronization is not limited to numerical models but constitutes a robust and reproducible feature of real-world weakly coupled chaotic networks.

VI. CONCLUSIONS

In this work, we have demonstrated that the route to synchronization in complex networks of chaotic oscilla-

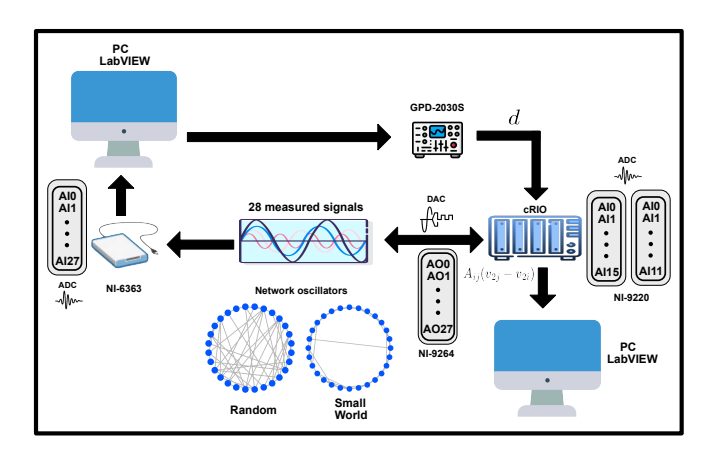


FIG. 7. Schematic of the hybrid experimental acquisition and feedback system. Electronic Rössler-like oscillators are interfaced to both a CompactRIO (cRIO-9074) embedded platform and a DAQ board (NI-6363) through their voltage outputs. The cRIO executes the real-time processing required to compute the diffusive coupling terms from the instantaneous node states and generates the feedback signals according to a prescribed adjacency matrix, while the global coupling strength d is adjusted via an analog control voltage supplied by a programmable power source (GPD-2030S). Signals are recorded through the DAQ for offline analysis and the whole setup is automated with LabVIEW. The hybrid (cRIO+DAQ) architecture enables precise, repeatable sweeps of d and flexible real-time implementation of different topologies.

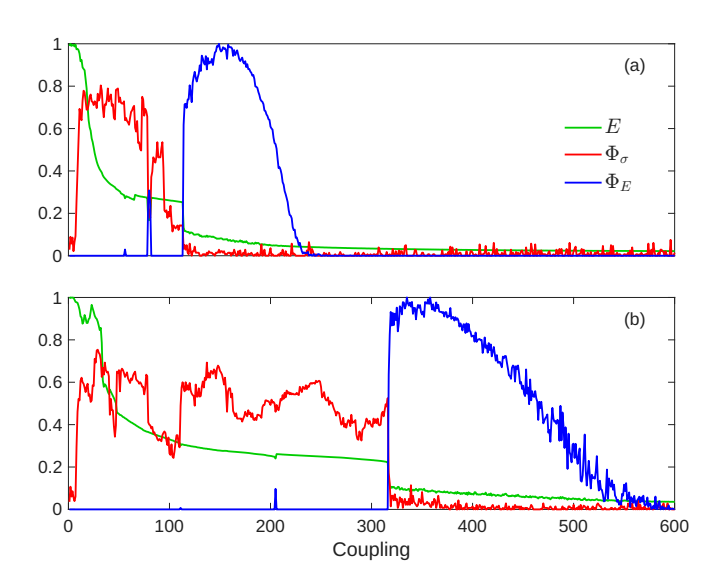


FIG. 8. Normalized mean synchronization error $\langle E \rangle$ (green), chaotic itinerancy index Φ_{β} (red) and synchronization index Φ_{E} (blue) in the experimental $N{=}28$, $\langle k \rangle{=}4$ networks with two different topologies: (a) Erdös-Renyi, (b) Watts-Strogatz with rewiring probability $p{=}0.1$. Analysis parameters: $N_{\beta} = 6$, D = 100, $\theta_{E} = 0.02$.

tors proceeds through two successive and distinct dynamical phenomena: chaotic itinerancy and intermittent synchronization. Although both phenomena have been previously reported, they are often treated as manifestations of the same underlying process. Our results clarify instead that CI and IS constitute mutually exclusive stages, each governed by distinct dynamical mechanisms and critical properties, and occurring in separate intervals of the coupling strength.

By introducing a symbolic dynamics, we provided a nodal characterization of CI as a collective yet unsynchronized exploration of metastable regimes that constitute each nodal sub-attractor. CI, which had not been systematically studied in heterogeneous networks, is shown to depend strongly on structural diversity: networks with broader degree distributions exhibit richer itinerant dynamics, and high-degree nodes have access to larger set of regimes than low-degree nodes. A symbolic functional synchronization analysis further shows that, during CI, nodes tend to synchronize their transitions before their regimes, highlighting a form of temporal coordination that precedes global coherence. The subsequent alignment of symbolic states marks the onset of IS before full synchronization.

As coupling increases, CI vanishes and gives rise to IS, where the network alternates irregularly between synchronous and desynchronous phases, displaying on-off intermittency. Both regimes exhibit power-law residence times, indicating that critical organization structures the entire synchronization route. The transition between these two phenomena occurs within a consistent coupling interval across network topologies and oscillator types. suggesting a robust and possibly general scenario. An analysis of the Lyapunov spectrum across this transition establishes a direct correspondence between the two phenomena and the hierarchical reduction of dimensionality that accompanies the emergence of collective order. The experimental implementation in electronic oscillator networks reproduces these features, confirming that the two-step sequence CI-IS is not only a theoretical construct but a generic route observed in real systems.

Beyond its theoretical relevance, the sequential organization of critical regimes identified here could be central to understanding flexible coordination in biological and artificial systems. In the brain, chaotic itinerancy and intermittent synchronization have been proposed as mechanisms for cognitive flexibility and information routing [4, 15]. Similarly, in reservoir computing and neuromorphic architectures, operating near the transition between chaotic itinerancy and intermittent synchronization may optimize computational capacity and adaptability [34–36].

Overall, our results provide a unified framework linking transient, metastable, and critical dynamics in complex networks and highlight the fundamental role of structural heterogeneity in shaping the route to synchronization.

- [1] J. M. Beggs and D. Plenz, Neuronal avalanches in neocortical circuits, Journal of Neuroscience 23, 11167 (2003).
- [2] W. L. Shew and D. Plenz, Criticality and dynamics of cortical networks, Nature Reviews Neuroscience 15, 779 (2013).
- [3] M. A. Muñoz, Colloquium: Criticality and dynamical scaling in living systems, Reviews of Modern Physics 90, 031001 (2018).
- [4] R. Calvo, C. Martorell, G. B. Morales, S. Di Santo, and M. A. Muñoz, Frequency-dependent covariance reveals critical spatiotemporal patterns of synchronized activity in the human brain, Physical Review Letters 133, 208401 (2024).
- [5] S. A. Kauffman, The Origins of Order: Self-Organization and Selection in Evolution (Oxford University Press, Oxford, 1993).
- [6] R. V. Solé and J. Bascompte, Self-Organization in Complex Ecosystems (Princeton University Press, 2006).
- [7] N. Bertschinger and T. Natschläger, Real-time computation at the edge of chaos in recurrent neural networks, Neural Computation 16, 1413 (2004).
- [8] G. Deco and M. L. Kringelbach, Metastability, multistability, and criticality in large-scale brain dynamics, Trends in Cognitive Sciences 25, 1065 (2021).
- [9] I. Tsuda, Dynamic link of memory—chaotic memory map in nonequilibrium neural networks, Neural Networks 5, 313 (1992).
- [10] L. M. Kay, A challenge to chaotic itinerancy from brain dynamics, Chaos 13, 1057 (2003).
- [11] V. P. Vera-Ávila, J. R. Sevilla-Escoboza, and I. Leyva, Complex networks exhibit intermittent synchronization, Chaos 30, 103119 (2020).
- [12] A. Choudhary, C. Mitra, V. Kohar, S. Sinha, and J. Kurths, Small-world networks exhibit pronounced intermittent synchronization, Chaos 27, 111101 (2017).
- [13] N. Platt, E. A. Spiegel, and C. Tresser, On-off intermittency: A mechanism for bursting, Physical Review Letters 70, 279 (1993).
- [14] J. F. Heagy, N. Platt, and S. M. Hammel, Characterization of on-off intermittency, Physical Review E 49, 1140 (1994).
- [15] M. Breakspear, Dynamic models of large-scale brain activity, Nature Neuroscience 20, 340 (2017).
- [16] F. S. Borges, E. C. Gabrick, P. R. Protachevicz, G. S. V. Higa, E. L. Lameu, P. X. R. Rodriguez, M. S. A. Ferraz, J. D. Szezech, A. M. Batista, and A. H. Kihara, Intermittency properties in a temporal lobe epilepsy model, Epilepsy & Behavior 139, 109072 (2023).
- [17] K. Kaneko and I. Tsuda, Chaotic itinerancy, Chaos 13, 926 (2003).
- [18] I. Tsuda, Chaotic itinerancy and its roles in cognitive neurodynamics, Current Opinion in Neurobiology 31, 67 (2015).
- [19] D. Koch, A. Nandan, G. Ramesan, and A. Koseska, Biological computations: Limitations of attractor-based formalisms and the need for transients, Biochemical and Biophysical Research Communications 720, 150069 (2024).
- [20] K. Kaneko, Clustering, coding, switching, hierarchical ordering, and control in a network of chaotic elements, Physica D: Nonlinear Phenomena 41, 137 (1990).

- [21] W. J. Freeman, Evidence from human scalp electroencephalograms of global chaotic itinerancy, Chaos 13, 1067 (2003).
- [22] K. Otsuka, Chaotic itinerancy in a coupled-element multistable optical chain, Physical Review A 43, 618 (1991).
- [23] R. Iwami, T. Mihana, K. Kanno, S. Sunada, M. Naruse, and A. Uchida, Controlling chaotic itinerancy in laser dynamics for reinforcement learning, Science Advances 8, eabn8325 (2022).
- [24] J.-J. Aucouturier, Y. Ogai, and T. Ikegami, Making a robot dance to music using chaotic itinerancy in a network of fitzhugh-nagumo neurons, in *International Conference on Neural Information Processing* (Springer, 2007) pp. 647–656.
- [25] S. Steingrube, M. Timme, F. Wörgötter, and P. Manoonpong, Self-organized adaptation of a simple neural circuit enables complex robot behaviour, Nature Physics 6, 224 (2010).
- [26] J. Park, H. Mori, Y. Okuyama, and M. Asada, Chaotic itinerancy within the coupled dynamics between a physical body and neural oscillator networks, PloS one 12, e0182518 (2017).
- [27] S. Recanatesi, U. Pereira-Obilinovic, M. Murakami, Z. Mainen, and L. Mazzucato, Metastable attractors explain the variable timing of stable behavioral action sequences, Neuron 110, 139 (2022).
- [28] T. Sasaki, N. Matsuki, and Y. Ikegaya, Metastability of active ca3 networks, Journal of Neuroscience 27, 517 (2007).
- [29] M. Morrison and L.-S. Young, Chaotic heteroclinic networks as models of switching behavior in biological systems, Chaos 32, 123102 (2022).
- [30] J. A. Roberts, L. L. Gollo, R. G. Abeysuriya, G. Roberts, P. B. Mitchell, M. W. Woolrich, and M. Breakspear, Metastable brain waves, Nature Communications 10, 1056 (2019).
- [31] P. Ashwin, M. Fadera, and C. Postlethwaite, Network attractors and nonlinear dynamics of neural computation, Current Opinion in Neurobiology 84, 102818 (2024).
- [32] F. Hancock, F. E. Rosas, A. I. Luppi, M. Zhang, P. A. M. Mediano, J. Cabral, G. Deco, M. L. Kringelbach, M. Breakspear, J. A. S. Kelso, and F. E. Turkheimer, Metastability demystified - the foundational past, the pragmatic present and the promising future, Nature Reviews Neuroscience 26, 82 (2025).
- [33] K. L. Rossi, R. C. Budzinski, E. S. Medeiros, B. R. Boaretto, L. Muller, and U. Feudel, Dynamical properties and mechanisms of metastability: A perspective in neuroscience, Physical Review E 111, 021001 (2025).
- [34] K. Inoue, K. Nakajima, and Y. Kuniyoshi, Designing spontaneous behavioral switching via chaotic itinerancy, Science Advances 6, 3989 (2020).
- [35] L.-W. Kong, G. A. Brewer, and Y.-C. Lai, Reservoircomputing based associative memory and itinerancy for complex dynamical attractors, Nature Communications 15, 4840 (2024).
- [36] J. O'Hagan, A. Keane, and A. Flynn, Confabulation dynamics in a reservoir computer: Filling in the gaps with untrained attractors, Chaos 35, 093130 (2025).
- [37] T. Kabayama, M. Komuro, Y. Kuniyoshi, K. Aihara, and K. Nakajima, Crisis-induced intermittency in reservoir

- computing, Physical Review Research 7, L032058 (2025).
- [38] A. Mattera, V. Alfieri, G. Granato, and G. Baldassarre, Chaotic recurrent neural networks for brain modelling: A review, Neural Networks 184, 107079 (2025).
- [39] S. Uchiyama and H. Fujisaka, Wandering behavior of the chaotic itinerancy in an oscillator neural network model, Progress of Theoretical Physics Supplement 161, 381 (2006).
- [40] J. J. Torres, J. Marro, J. M. Cortes, and B. Wemmenhove, Instabilities in attractor networks with fast synaptic fluctuations and partial updating of the neurons activity, Neural Networks 21, 1272 (2008).
- [41] A. A. Khatun, Y. A. Muthanna, N. Punetha, and H. H. Jafri, Collective dynamics of coupled lorenz oscillators near the hopf boundary: Intermittency and chimera states, Physical Review E 109, 034208 (2024).
- [42] T. Sameshima, K. Fukushima, H. Shibata, and T. Yamada, Lyapunov spectrum analysis for a chaotic transition phenomenon, Europhysics Letters **62**, 21 (2003).
- [43] M. Timme, F. Wolf, and T. Geisel, Prevalence of unstable attractors in networks of pulse-coupled oscillators, Physical Review Letters 89, 154105 (2002).
- [44] D. J. Gauthier and J. C. Bienfang, Intermittent loss of synchronization in coupled chaotic oscillators: Toward a new criterion for high-quality synchronization, Physical Review Letters 77, 1751 (1996).
- [45] S. Boccaletti and D. Valladares, Characterization of intermittent lag synchronization, Physical Review E 62, 7497 (2000).
- [46] A. Choudhary, C. Mitra, V. Kohar, S. Sinha, and J. Kurths, Small-world networks exhibit pronounced intermittent synchronization, Chaos 27, 111101 (2017).
- [47] G. Benettin, L. Galgani, A. Giorgilli, and J.-M. Strelcyn, Lyapunov characteristic exponents for smooth dynamical systems and for hamiltonian systems; a method for computing all of them. part 1: Theory, Meccanica 15, 9 (1980).
- [48] R. Gutiérrez, R. Sevilla-Escoboza, P. Piedrahita, C. Finke, U. Feudel, J. M. Buldú, G. Huerta-Cuellar,

- R. Jaimes-Reátegui, Y. Moreno, and S. Boccaletti, Generalized synchronization in relay systems with instantaneous coupling, Physical Review E 88, 052908 (2013).
- [49] J. Kaplan and J. Yorke, Chaotic behavior of multidimensional difference equations, Lecture Notes in Mathematics 730, 204 (1979).
- [50] K. Kaneko, Information cascade with marginal stability in a network of chaotic elements, Physica D: Nonlinear Phenomena 77, 456 (1994).
- [51] I. Tsuda, H. Fujii, S. Tadokoro, T. Yasuoka, and Y. Yamaguti, Chaotic itinerancy as a mechanism of irregular changes between synchronization and desynchronization in a neural network, Journal of integrative neuroscience 3, 159 (2004).
- [52] G. Tirabassi, R. Aristides, C. Masoller, and D. J. Gauthier, Bubbling in oscillator networks, arXiv preprint arXiv:2504.07374 (2025).
- [53] J. Namikawa, Chaotic itinerancy and power-law residence time distribution in stochastic dynamical systems, Physical Review E 72, 026204 (2005).
- [54] H. Fujisaka and T. Yamada, Stability Theory of Synchronized Motion in Coupled-Oscillator Systems, Progress of Theoretical Physics 69, 32 (1983).
- [55] P. W. Hammer, N. Platt, S. M. Hammel, J. F. Heagy, and B. D. Lee, Experimental observation of on-off intermittency, Physical Review Letters 73, 1095 (1994).
- [56] S. C. Venkataramani, T. M. Antonsen, E. Ott, and J. C. Sommerer, Characterization of on-off intermittent time series, Physics Letters A 207, 173 (1995).
- [57] A. Tlaie, I. Leyva, R. Sevilla-Escoboza, V. P. Vera-Avila, and I. Sendiña Nadal, Dynamical complexity as a proxy for the network degree distribution, Physical Review E 99, 012310 (2019).
- [58] C. Letellier, I. Sendiña-Nadal, L. Minati, and I. Leyva, Node differentiation dynamics along the route to synchronization in complex networks, Physical Review E 104, 014303 (2021).
- [59] D. J. Watts and S. H. Strogatz, Collective dynamics of 'small-world'networks, Nature 393, 440 (1998).